J Stat Phys (2007) 129: 453–468
DOI 10.1007/s10955-007-9392-z

Critical Behavior of the Blume-Emery-Griffiths Model for a Simple Cubic Lattice on the Cellular Automaton

N. Seferoğlu · B. Kutlu

Received: 16 May 2007 / Accepted: 1 August 2007 / Published online: 13 September 2007

Abstract The spin-1 Ising model with the nearest-neighbour bilinear and biquadratic interactions and single-ion anisotropy is simulated on a cellular automaton which improved from the Creutz cellular automaton (CCA) for a simple cubic lattice. The simulations have been made for several $k = K/J$ and $d = D/J$ in the $0 \leq d < 3$ and $-2 \leq k \leq 0$ parameter regions. We confirm the existence of the re-entrant and the successive re-entrant phase transitions near the phase boundary. The phase diagrams characterizing phase transitions are presented for comparison with those obtained from other calculations. The static critical exponents are estimated within the framework of the finite-size scaling theory at $d = 0$, 1 and 2 in the interval $-2 \leq k \leq 0$. The results are compatible with the universal Ising critical behavior.

Keywords Spin-1 Ising model · Creutz cellular automaton · Re-entrant phase transition · Simple cubic lattice

1 Introduction

The Hamiltonian of the Blume-Emery-Griffiths (BEG) model [1] is given by,

$$H_I = -J \sum_{\langle ij \rangle} S_i S_j - K \sum_{\langle ij \rangle} S_i^2 S_j^2 - D \sum_i S_i^2 \tag{1}$$

where $S_i = \pm 1, 0$ and $\langle ij \rangle$ denotes summation over all nearest-neighboring (nn) spin pairs on a simple cubic lattice. The parameters J and K are the bilinear and biquadratic interaction energies, respectively and D is the single-ion anisotropy constant. The model was originally

N. Seferoğlu (✉)
Fen Bilimleri Enstitüsü, Fizik Anabilim Dalı, Gazi Üniversitesi, Ankara, Turkey
e-mail: nurguls@gazi.edu.tr

B. Kutlu
Fen-Edebiyat Fakültesi, Fizik Bölümü, Gazi Üniversitesi, 06500 Teknikokullar, Ankara, Turkey
e-mail: bkutlu@gazi.edu.tr

introduced to describe the phase separation and superfluidity in the He^3–He^4 mixtures and was used to describe multicomponent fluids [2, 3], microemulsions [4], and semiconductors alloys [5], etc.

The model has been extensively studied by different techniques; the mean-field approximation (MFA) [1–3, 6–8], renormalization group theory [9, 10], effective-field theory [11, 12], Monte Carlo simulations [13–16]. Besides these methods, the BEG model has been studied by other techniques such as the Monte Carlo renormalization group [17], cluster variation method [18–21], Bethe approximation [15], and cellular automaton [22–24]. Most of these analysis predict that the phase diagrams of the BEG model include a variety of interesting features. The global phase diagram of the model on three dimension for $K < 0$ was obtained by MFA [7], showing a variety of interesting features, including single and double re-entrancy region and ferrimagnetic phases. On the other hand, a full phase diagram of the model was constructed in the full J-K-D parameter space by the Bethe approximation and several kinds of phase transitions, such as successive, re-entrant and double re-entrant transitions, were obtained [15]. These transitions are also confirmed by Monte Carlo simulations on a simple cubic lattice at certain interaction parameters and the critical exponent ν is estimated by use the size dependence of Binder cumulant for some special values of parameters [15]. However, there is no extensive analysis within the framework of the finite-size scaling theory to determine the static critical exponents (α, β, γ, and ν).

In this paper we studied the three-dimensional BEG model using an improved heating algorithm from the Creutz Cellular Automaton (CCA). Particularly, our interest is focused to study the re-entrant behavior of the BEG model in the case of $K/J \leq 0$ ($J > 0$) near the ferromagnetic phase (F) and the stagger quadrupolar (SQ) phase boundary and obtain the universality of the model in this region. For this purpose, the temperature variations of the two-sublattice order parameters (m_A, m_B and q_A, q_B), the susceptibility (χ) and the specific heat (C) are computed on a simple cubic lattice. The static critical exponents are estimated by analyzing the data within the framework of finite-size scaling theory. The CCA algorithm is a microcanonical algorithm interpolating between the conventional Monte Carlo and molecular dynamics techniques on a cellular automaton, and it was first introduced by Creutz [25]. In the previous papers [22–32], the CCA algorithm and improved algorithms from CCA were used to study the critical behavior of the different Ising model Hamiltonians on the two, three and higher-dimensions. It was shown that they have successfully produced the critical behavior of the models. The BEG model on a three dimensional lattice is expected to be in universality class of the three dimensional Ising model with the critical exponents $\alpha = 0.12$, $\beta = 0.31$, $\gamma = 1.25$, and $\nu = 0.64$. The remainder of the paper is organized as follows. The details of the model is explained in Sect. 2, the results are discussed in Sect. 3 and a conclusion is given in Sect. 4.

2 Model

Three variables are associated with each site of the lattice. The value of each sites are determined from its value and those of its nearest-neighbors at the previous time step. The updating rule, which defines a cellular automaton, is as follows: Of the three variables on each site, the first one is Ising spin B_i. Its value may be 0 or 1 or 2. The Ising spin energy for the model is given by (1). In (1), $Si = Bi - 1$. The second variable is for momentum variable conjugate to the spin (the demon). The kinetic energy associated with the demon, H_k, is an integer, which equal to the changing in the Ising spin energy for the any spin flip

and its values lie in the interval $(0, r)$. The upper limit of the interval, r, takes a different value for each (J, K, D) parameter set. The total energy

$$H = H_I + H_K \tag{2}$$

is conserved. For a given total energy the system temperature is obtained from the average value of kinetic energy, which is given by:

$$\langle H_K \rangle = \frac{\sum_{n=0}^{r} n e^{-nJ/kT}}{\sum_{n=0}^{r} e^{-nJ/kT}}. \tag{3}$$

The expectation value in (3) is a average over the lattice and the number of the time steps.

The third variable provides a checkerboard style updating, and so it allows the simulation of the Ising model on a cellular automaton. The black sites of the checkerboard are updated and then their color is changed into white; white sites are changed into black without being updated. The updating rules for the spin and the momentum variables are as follows: For a site to be updated its spin is changed one of the other two states with $1/2$ probability and the change in the Ising spin energy, dH_I is calculated. If this energy change is transferable to or from the momentum variable associated with this site, such that the total energy H is conserved, then this change is done and the momentum is appropriately changed. Otherwise the spin and the momentum are not changed. Because of the third variable, the algorithm requires two time steps to give every spin of the lattice a chance to change. Thus, in comparison to ordinary Monte Carlo simulations, two steps correspond to one full sweep over the system variables.

The heating algorithm is divided into two basic parts, initialization procedure and the taking of measurements. In the initialization procedure, firstly, all spins in the lattice sites take the ferromagnetic ordered structure or staggered quadrupole ordered structure according to selected (J, K, D) parameter set and the kinetic energy per site which is equal to the maximum change in the Ising spin energy for the any spin flip is given to the certain percent of the lattice via the second variables. This configuration is run during the 10 000 cellular automaton time steps. At the end of the this step, the configuration in the ordered structure at the low temperature is obtained. In the next steps last configuration in the ordered structure has been chosen as a starting configuration for the heating run. Rather than resetting the starting configuration at each energy, it is used the final configuration at a given energy as the starting point for the next. During the heating cycle, energy is added to the spin system through the second variable of each site (H_k) after 1 000 000 cellular automaton steps. This process is realized by increasing of 3% in the kinetic energy of each site. This means that the increasing value of H_k is obtained from the integer part of the $0.03 H_k$.

3 Results and Discussion

The simulations are carried on simple cubic lattice $L \times L \times L$ of the linear dimensions $L = 12$, 16, 18, and 24 with periodic boundary conditions. The computed values of the quantities are averages over the lattice and over the number of time steps (1 000 000) with discard of the first 100 000 time steps during which the cellular automaton develops.

The various phases of the model for $J > 0$ are defined according to the values of the two sublattice $m_A \equiv \langle S_i \rangle_A$, $m_B \equiv \langle S_i \rangle_B$, $q_A \equiv \langle S_i^2 \rangle_A$, $q_B \equiv \langle S_i^2 \rangle_B$, where the subscript A and B refer to the two sublattice: ferromagnetic phase (F): $m_A = m_B \neq 0$, $q_A = q_B$; quadrupolar phase (Q): $m_A = m_B = 0$, $q_A = q_B$; staggered quadrupolar phase (SQ): $m_A = m_B = 0$, $q_A \neq q_B$; ferrimagnetic phase (FI): $m_A \neq m_B \neq 0$, $q_A \neq q_B$.

The temperature dependence of the sublattice order parameters (m_A, m_B, q_A and q_B) are studied to determine the types of the phase transitions for $0 \leq d = D/J < -3$ and $-2 \leq k = K/J \leq 0$ parameter region. For the reproduce of the phase diagrams using CCA simulations, the finite critical temperature ($t = k_B T/zJ$) are estimated from the maxima of the specific heat on the lattice with $L = 18$. On the other hand, the critical temperature values for the finite-size scaling analysis are estimated from the temperature variation of the Binder cumulant [33, 34]. The Binder cumulant is given by

$$g_L = 1 - \frac{\langle m^4 \rangle}{3\langle m^2 \rangle^2}. \tag{4}$$

The critical exponents ν can be estimated using the finite-size scaling relation for the Binder cumulant, which is defined by [34]

$$g_L = G(\varepsilon L^{1/\nu}) \tag{5}$$

where $\varepsilon = (T - Tc(\infty))/Tc(\infty)$.

The finite-size scaling relations of the order parameter m, susceptibility χ and specific heat C are given by

$$m = L^{-\beta/\nu} X(\varepsilon L^{1/\nu}) \tag{6}$$

$$kT\chi = L^{\gamma/\nu} Y(\varepsilon L^{1/\nu}) \tag{7}$$

$$C = L^{\alpha/\nu} Z(\varepsilon L^{1/\nu}). \tag{8}$$

For large $x = \varepsilon L^{1/\nu}$, the infinite lattice critical behaviors must be asymptotically reproduced, that is,

$$X(x) = Ax^{\beta} \tag{9}$$

$$Y(x) = Bx^{-\gamma} \tag{10}$$

$$Z(x) = Cx^{-\alpha}. \tag{11}$$

The ground state phase diagram of the BEG model on the (d, k) plane is shown in Fig. 1. It is shown that the ground state phase diagram of the model has ferromagnetic (F), perfect zero (PZ) and staggered quadrupole (SQ) ordering region [15]. The calculations are done in the F and SQ phase region for $d = 0$, 1 and 2 in the interval $-2 \leq k \leq 0$. The types of phase transition (PT) obtained from the CCA calculations are also shown in Fig. 1. The second order $Q \to F$ PTs and $Q \to SQ$ PTs occur for certain d and k values in the F and SQ ordering region, respectively. However, the re-entrant $Q \to F \to Q \to SQ$ PTs and successive $Q \to F \to SQ$ PTs take place for some values of the d and k parameters near the phase boundary. The phase diagram on the (k, t) plane for $d = 0$, 1 and 2 in the interval $-2 \leq k \leq 0$ are shown in Fig. 2. The similar behavior is seen in the phase diagrams obtained within the Bethe approximation [15] for $z = 6$ and the effective field theory [12] for $z = 3$ on the (k, t) plane. As it is seen from Fig. 2, the model has a bicritical point (BCP) at which two second order lines meet on the first order line. The bicritical point coordinates on a finite lattice with $L = 18$ are shown in Table 1.

In this parameter region, the model exhibits several kinds of phase transitions (PTs) as described in following:

(i) Second order $Q \to F$ PTs when $d = 0$ and $k \geq -1$, $d = 1$ and $k \geq -1.16$ or $d = 2$ and $k \geq -1.33$.

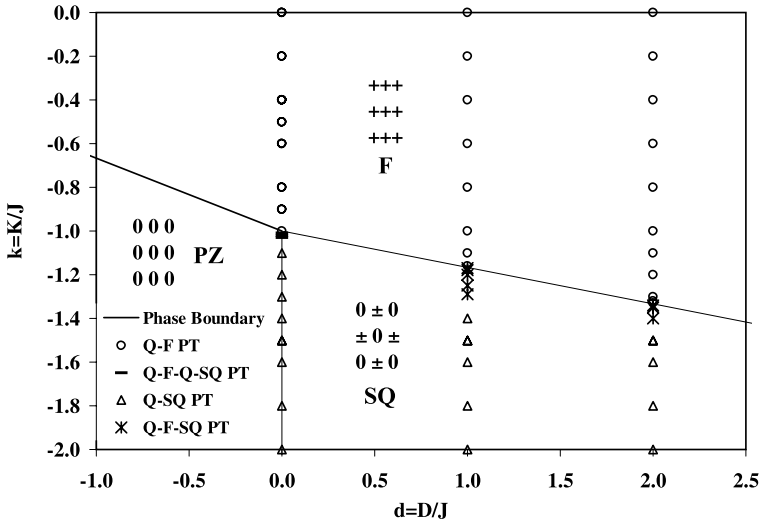

Fig. 1 The phase diagram (d–k plane) in the ground state and the types of phase transitions obtained on a simple cubic lattice

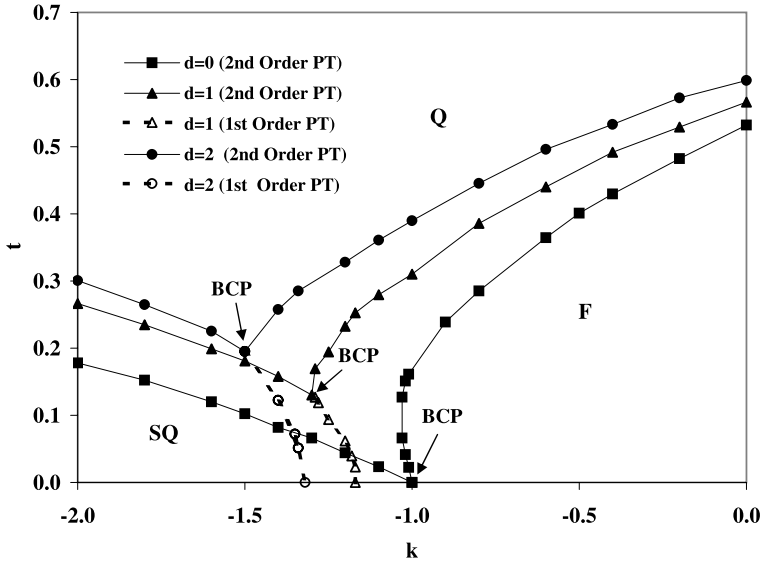

Fig. 2 The phase diagram in the (k, t) plane for $d = 0$, 1 and 2 in the interval $-2 \leq k \leq 0$

Table 1 The bicritical point values of (k, t) phase diagrams for several d values on a finite lattice with $L = 18$

d	k	t
0	-1	0
1	-1.29	0.17 ± 0.02
2	-1.5	1.20 ± 0.03

(ii) Re-entrant $Q \to F \to Q \to SQ$ PTs when $d = 0$ and $-1.04 < k < -1$.
(iii) Successive $Q \to F \to SQ$ PTs occur when $d = 1$ and $-1.3 < k \leq -1.16$ or $d = 2$ and $-1.5 < k \leq -1.3$.
(iv) Second order $Q \to SQ$ PTs when $d = 1$ and $k \leq -1.3$ or $d = 2$ and $k \leq -1.5$.

For a selected d and k values, the behavior of the thermodynamic quantities for above-mentioned phase transitions and the universality of the model are given in the following:

3.1 $Q \to F$ Phase Transition

The order parameters and the susceptibility obtained at $d = 0$ for different values of k are shown in Fig. 3a and b. There is the second order PT from quadrupolar phase to ferromagnetic phase ($Q \to F$). At the same time, the susceptibility data shows characteristic peaks at the critical temperature as expected for a second order phase transition. However, the value of magnetization for $k = -1$ at zero temperature is lower than the magnetization for the $k > -1$ values. In the ground state, the ferromagnetic, perfect zero and staggered quadrupolar phases meet at the point with the coordinate $d = 0$, $k = -1$. At $d = 0$ for $k = -1$ the temperature variations of the Binder cumulant are illustrated in Fig. 4a for different lattice sizes. The estimated critical temperature value from the intersection of the Binder cumulant curves for the different lattice sizes is 1.098 ± 0.018 at this point. This result is in agreement with MC study [16] but is much lower than the mean field prediction [7]. The scaling of the Binder cumulant for this point is shown in Fig. 4b. It can be seen from figure that the scaling data for the finite-size lattices lie on a single curve near the critical temperature when the value of the correlation length critical exponent is equal to the universal value of $\nu = 0.64$. The scaling of the Binder cumulant at $d = 0$ for $k \geq -1$ exhibits a similar behavior with $\nu = 0.64$. However the finite-size scaling plots of the data for the order parameter m and

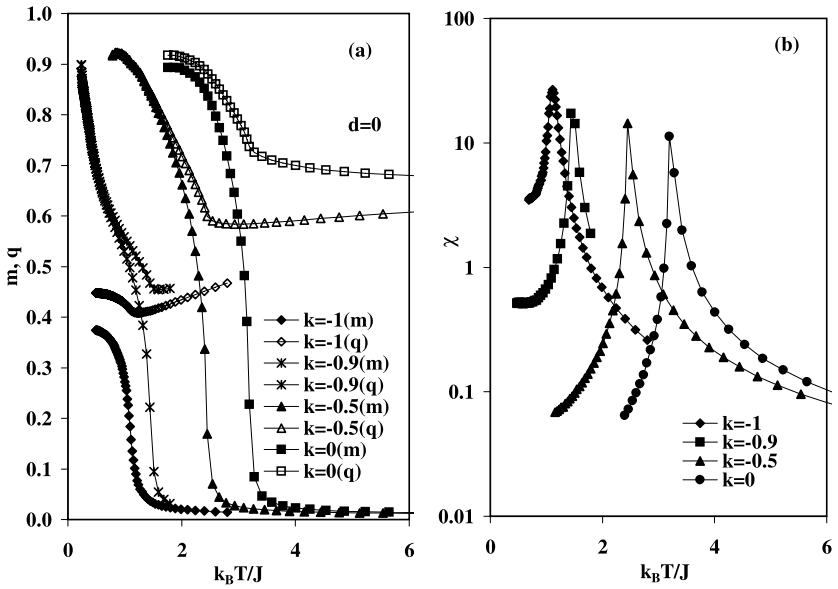

Fig. 3 The temperature dependence of **a** the order parameters m and q, **b** the susceptibility χ at $d = 0$ for different values of k on a lattice with $L = 18$

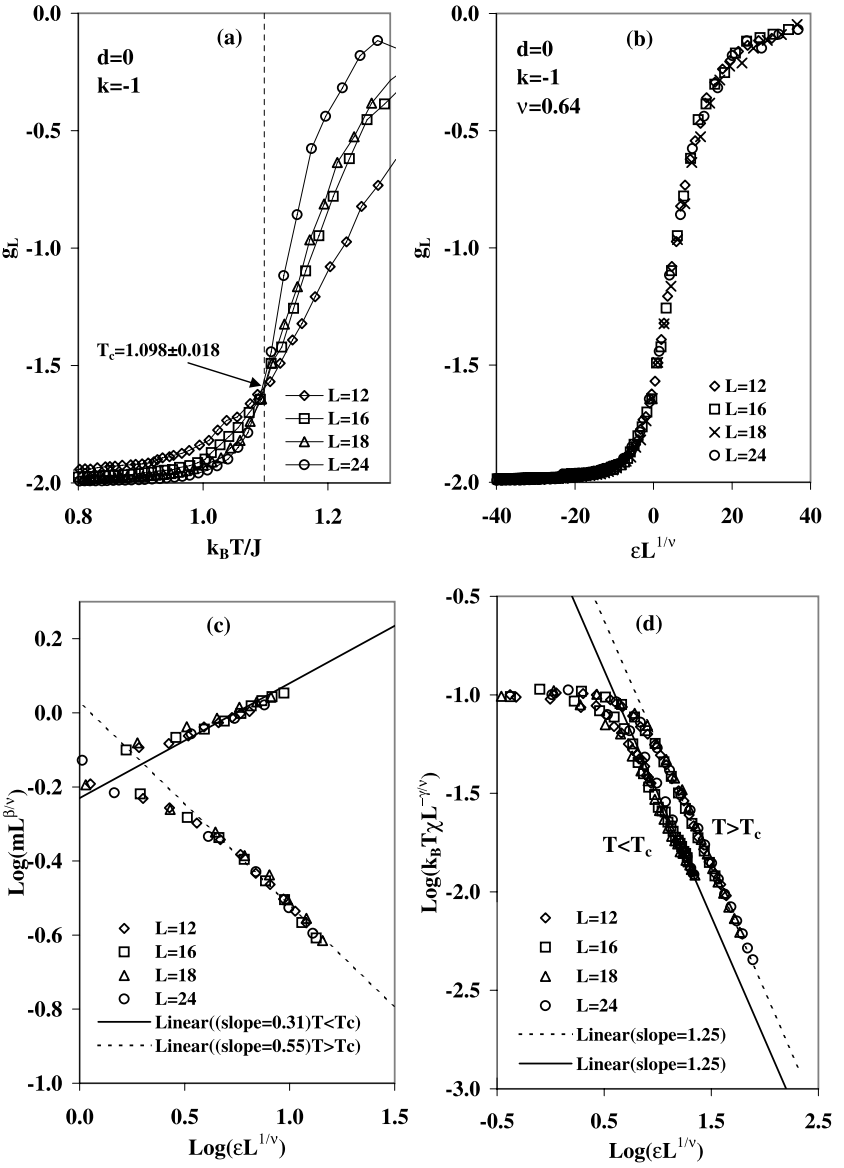

Fig. 4 At $d = 0$ for $k = -1$ **a** the Binder cumulant as a function of k_BT/J, **b** finite size scaling plots of the Binder cumulant with $\nu = 0.64$, **c** finite size scaling plots of order parameter, **d** finite size scaling plots of the magnetic susceptibility, $\varepsilon = |T - T_c|/T_c$ for $T < T_c$ and $\varepsilon = |T - T_c|/T$ for $T > T_c$

susceptibility are shown in Fig. 4c and d for this point. The data of the order parameter lie on a single curve for the temperature both below and above critical temperature with $\beta = 0.31$ and $\nu = 0.64$. Thus, the data for m are in agreement with the universal value of $\beta = 0.31$ for $T < T_c$. The straight line passing through the data for $T > T_c$ behaves according to (9) with $\beta' = 0.55$. The scaling of the susceptibility data also agrees with the asymptotic form with the critical exponents $\gamma = \gamma' = 1.25$ and $\nu = 0.64$ for both $T < T_c$ and $T > T_c$ at $d = 0$ for

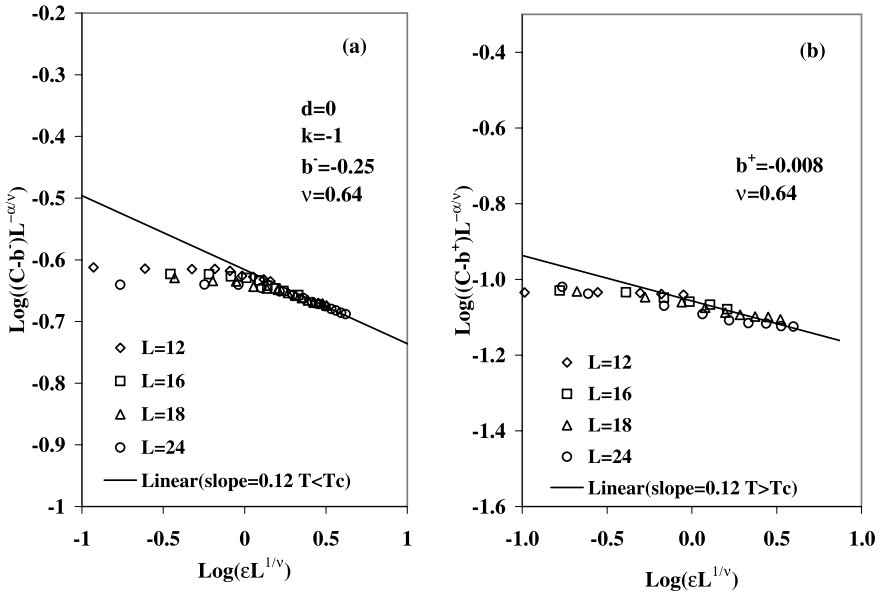

Fig. 5 At $d = 0$ for $k = -1$ **a** finite size scaling plots of the specific heat for $T < T_c$, **b** finite size scaling plots of the specific heat for $T > T_c$

$k \geq -1$. Furthermore, the finite size scaling plots of the singular portion of the specific heat ($C/k - b^{\pm}$) are shown in Fig. 5. The scaling data of the specific heat lies on a single curve with the value of $\alpha = \alpha' = 0.12$ for $T > T_c$ and $T < T_c$ at $d = 0$ for $k = -1$. The data of the specific heat obtained at $d = 0$ for $k > -1$ scales with $\alpha = \alpha' = 0.12$ and $\nu = 0.64$ for $T < T_c$ and $T > T_c$.

3.2 Re-entrant $Q \rightarrow F \rightarrow Q \rightarrow SQ$ Phase Transition

The sublattice order parameters obtained at $d = 0$ for $k = -1.01$, -1.02, -1.03 and -1.04 are shown in Fig. 6a. In the interval $-1.04 < k < -1$, the re-entrant $Q \rightarrow F \rightarrow Q \rightarrow SQ$ PTs take place and order parameters exhibit a continuous behavior at these transitions. On the other hand, the data of the susceptibility shows the two peaks which belong the $Q \rightarrow F$ and $F \rightarrow Q$ PTs (Fig. 6b). In addition, the specific heat has also no sign of the singularity which belongs to the lower transition $Q \rightarrow SQ$ PT (Fig. 7a). The lower transition $Q \rightarrow SQ$ occurs at extremely low temperature and looks a continuous transitions from the temperature dependence of the order parameters q_A and q_B. However, the Bethe approximation [15] indicates the existence of the three peaks for the $Q \rightarrow F \rightarrow Q \rightarrow SQ$ PT but there is only a peak belongs to the $Q \rightarrow SQ$ PT in the MC simulations [15]. Moreover, the specific heat has no characteristic behavior of the second order phase transition for the $Q \rightarrow F \rightarrow Q \rightarrow SQ$ PTs as indicated in the MC simulations [15]. Therefore it is important to obtain the critical exponents for these transitions.

On the other hand, according to the Bethe approximation [15], the re-entrant $Q \rightarrow F \rightarrow Q \rightarrow SQ$ PTs take place at $d = 0$ for $-1.05 < k < -1$. But, it is obtained that there is only $Q \rightarrow SQ$ PT occurs at $d = 0$ for $k \leq -1.04$. As seen from Fig. 7b, the order (F state) in the intermediate temperature at $d = 0$ for $k = -1.04$ shows the size-dependency and decreases

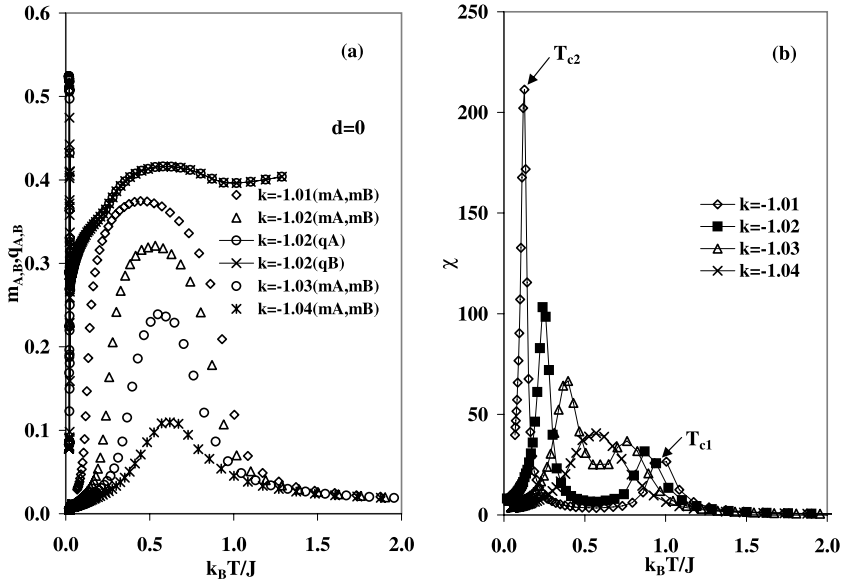

Fig. 6 The temperature dependence of **a** the sublattice order parameters m_A, m_B and q_A, q_B, **b** the susceptibility χ at $d = 0$ for $k = -1.01$, -1.02, -1.03 and -1.04 on a lattice with $L = 18$

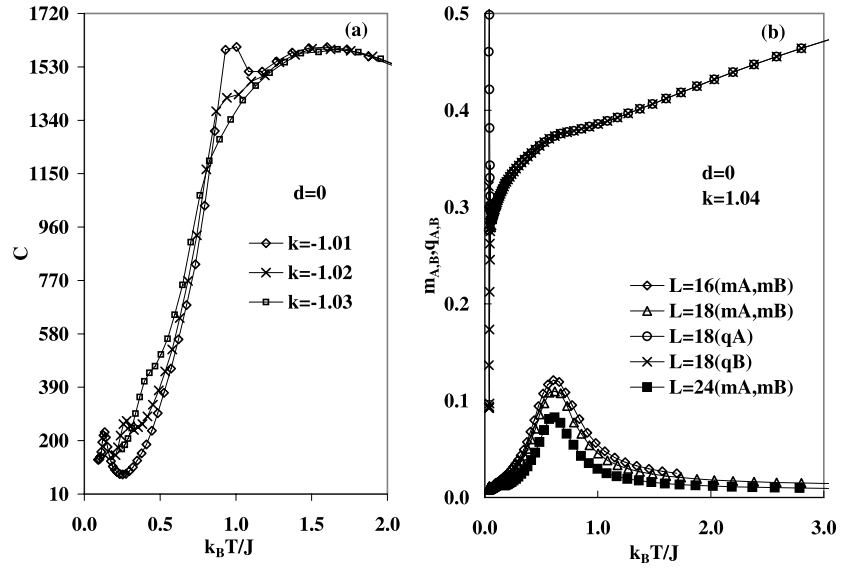

Fig. 7 The temperature dependence of the **a** specific heat C at $d = 0$ for $k = -1.01$, -1.02, -1.03 on a lattice with $L = 18$, **b** sublattice order parameters m_A, m_B and q_A, q_B at $d = 0$, $k = -1.04$ on $L = 16$, 18, 24

with the increasing lattice size. In addition, the susceptibility has no singularities belong to the $Q \to F \to Q$ PT (Fig. 6b).

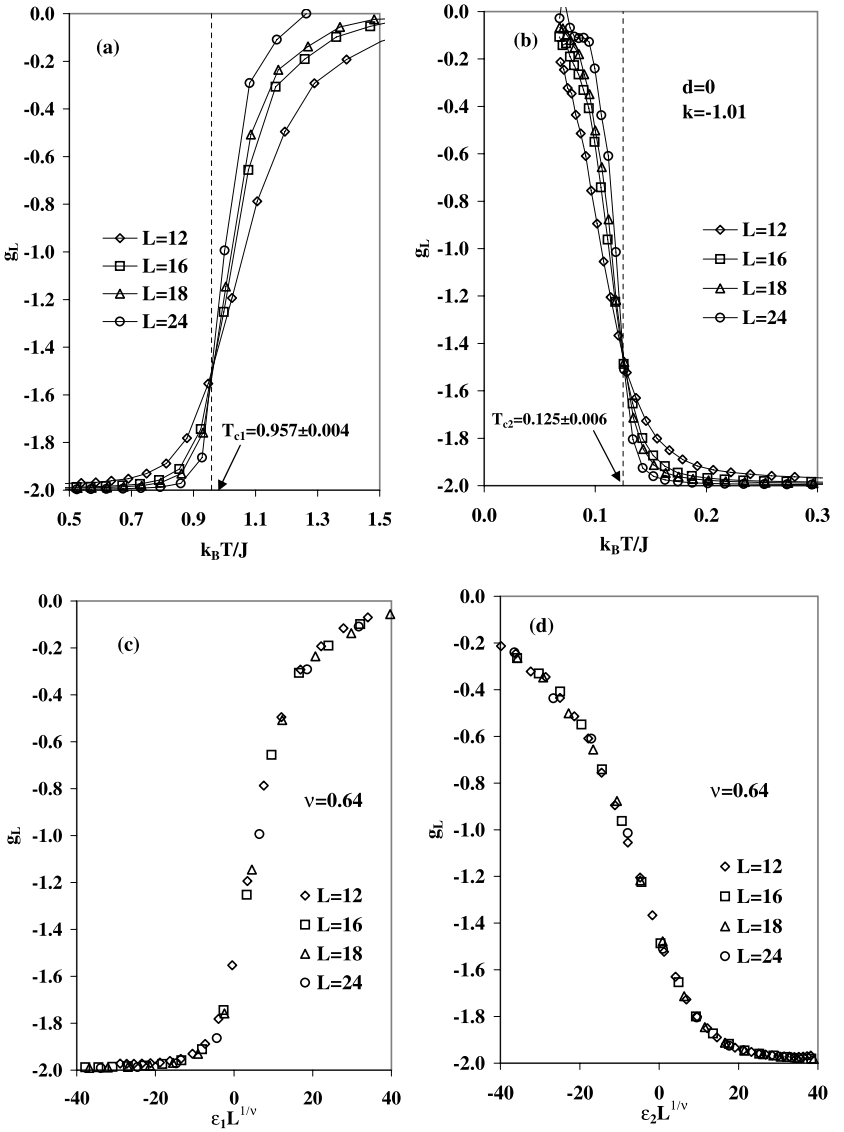

Fig. 8 At the re-entrant $Q \to F \to Q \to SQ$ PT, the Binder cumulant as a function of k_BT/J for the **a** $Q \to F$ PT **b** $F \to Q$ PT and the finite size scaling plots of the Binder cumulant with $\nu = 0.64$ for the **c** $Q \to F$ PT, $\varepsilon_1 = |(T - T_{c1})|/T_{c1}$, **d** $F \to Q$ PT, $\varepsilon_2 = |(T - T_{c2})|/T_{c2}$, at $d = 0$, $k = -1.01$

At $d = 0$ for $k = -1.01$, the temperature variations of the Binder cumulants for different lattice sizes which belong to the $Q \to F$ and $F \to Q$ transitions are given in Fig. 8a and b, respectively. The critical exponent ν for both of these transitions are estimated from the scaling of the Binder cumulant (Fig. 8c and d). Its value is equal to 0.64 for $-1.04 < k < -1$. Similarly, the estimated values of β and γ agrees with the universal values $\beta = 0.31$ and $\gamma = \gamma' = 1.25$ for $Q \to F$ and $F \to Q$ transition (Fig. 9).

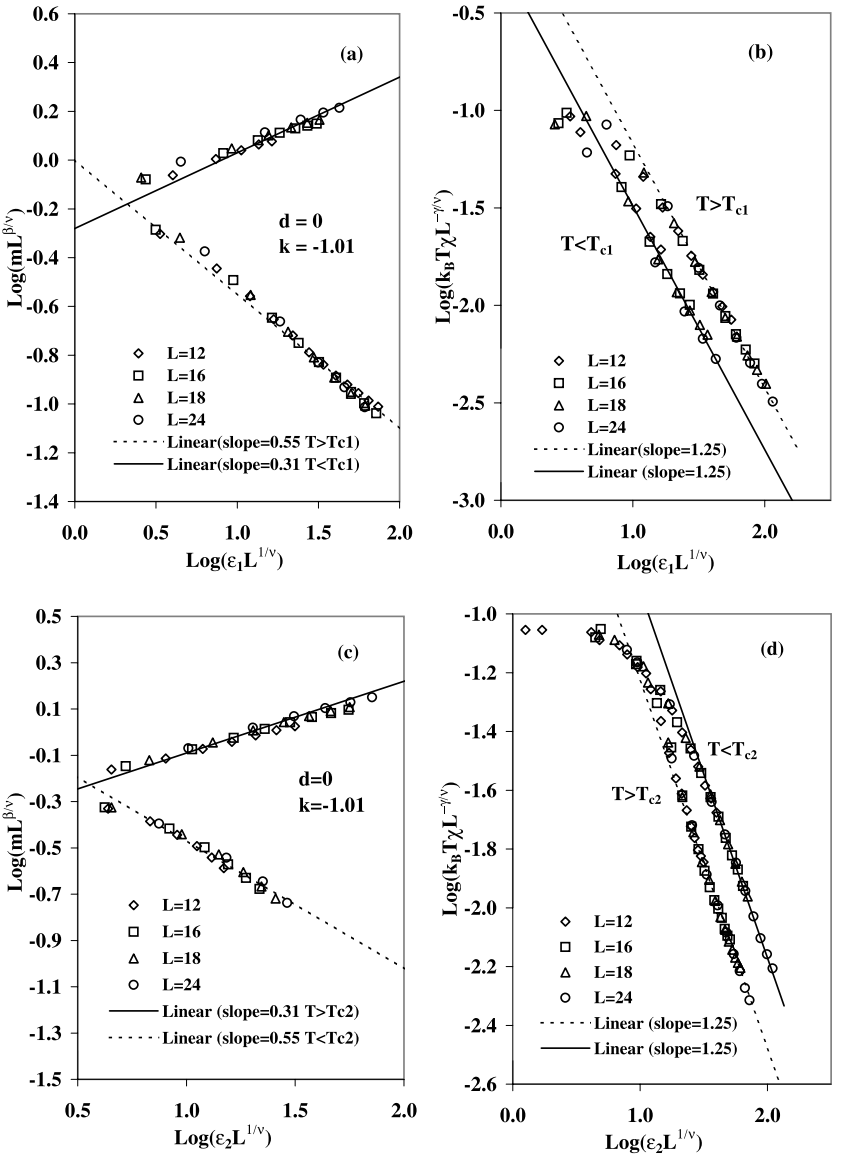

Fig. 9 At the re-entrant $Q \rightarrow F \rightarrow Q \rightarrow SQ$ PT, the finite size scaling plots of the **a** order parameter, **b** magnetic susceptibility, $\varepsilon_1 = |T - T_{c1}|T_{c1}$ for $T < T_{c1}$ and $T > T_{c1}$, for the $Q \rightarrow F$ PT, **c** order parameter, **d** magnetic susceptibility, $\varepsilon_2 = |T - T_{c2}|T$ for $T < T_{c1}$ and $T > T_{c1}$, for the $F \rightarrow Q$ PT

3.3 Successive Q → F → SQ Phase Transition

The sublattice order parameters and susceptibility are shown in Fig. 10a and b at $d = 1$ for $k = -1.2$. It is seen that, the order parameters exhibit a continuous behavior and the susceptibility has a characteristic peak for the higher transition $Q \rightarrow F$. However, the lower transition $F \rightarrow SQ$ is of the first order because the jump of the order parameters appear and

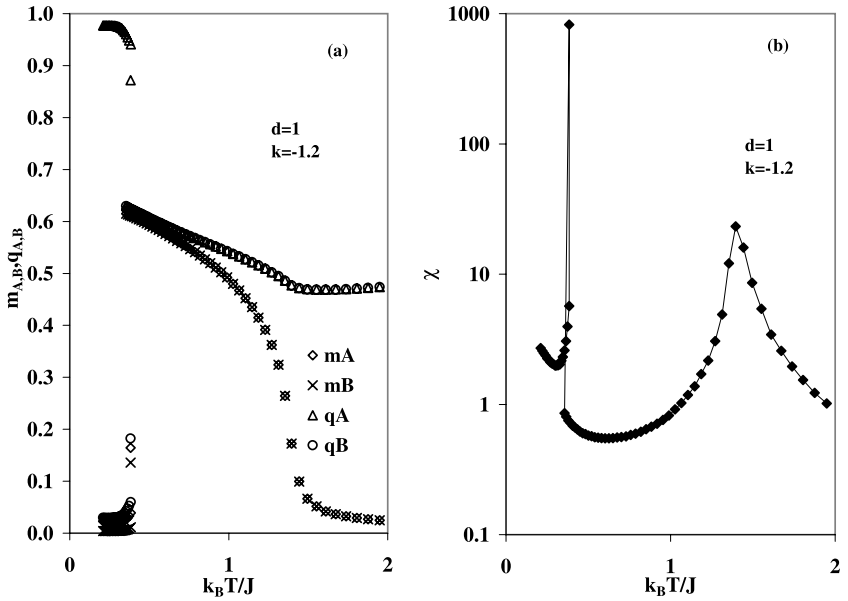

Fig. 10 The temperature dependence of **a** the sublattice order parameters m_A, m_B and q_A, q_B, **b** the susceptibility χ for $d = 1$ for $k = -1.2$ on a lattice with $L = 18$

the susceptibility shows a sharp peak at the transition temperature. The calculated specific heat indicates the existence of two peaks belongs to the higher transition $Q \to F$ and the lower transition $F \to SQ$ which is not shown here.

The estimated exponents are $\nu = 0.64$, $\beta = 0.31$, $\gamma = \gamma' = 1.25$ and $\alpha = 0.12$ for the higher transition $Q \to F$ from the finite-size scaling theory (Fig. 11).

3.4 Q → SQ Phase Transition

The temperature dependence of the sublattice order parameters at $d = 1$ for $k = -1.4, -1.8$ and -2 are shown in Fig. 12. The value of the order parameters m_A and m_B are equal to zero at below and above critical temperature for the $Q \to SQ$ transitions. Therefore the susceptibility has no information about the transition. But the temperature dependence of the internal energy is continuous and the specific heat shows a peak at the critical temperature at the $Q \to SQ$ transitions (Fig. 13).

4 Conclusion

The BEG model is simulated using the heating algorithm of the cellular automaton for simple cubic lattice. It is shown that, the model exhibits only the $Q \to F$ and $Q \to SQ$ PT in the ferromagnetic (F) and staggered quadrupolar (SQ) phase, respectively. However, the re-entrant and successive re-entrant PTs occur for some values of k and d parameters near the F and SQ phase boundary as expected. We have reconstructed the (k, t) phase diagrams for $d = 0$, 1 and 2 in the interval $-2 \leq k \leq 0$. To determine the universality of the model,

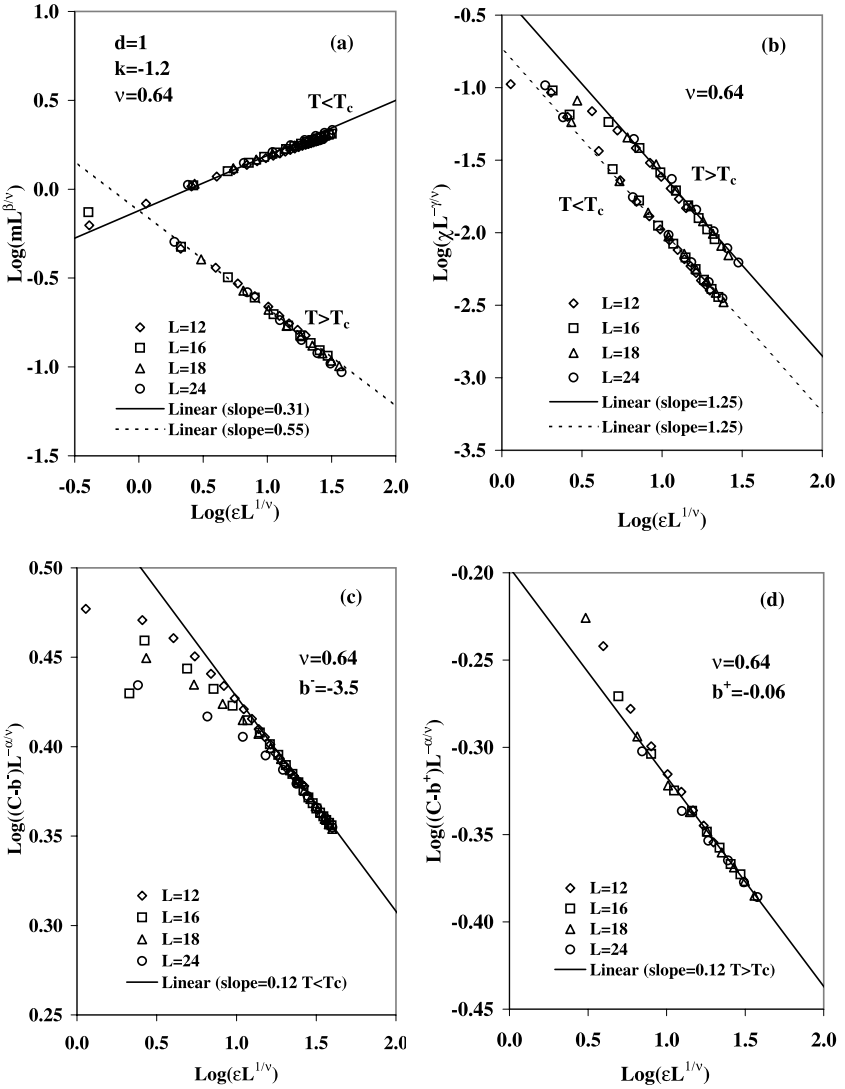

Fig. 11 At the successive $Q \to F \to SQ$ PT, the finite size scaling plots of the **a** order parameter, **b** magnetic susceptibility, $\varepsilon = |T - T_c|T_c$ for $T < T_c$ and $\varepsilon = |T - T_c|T$ for $T > T_c$, **c** specific heat for $T < T_c$, **d** specific heat for $T > T_c$, at $d = 1$, $k = -1.2$, for $Q \to F$ PT

the static critical exponents (α, β, γ) are estimated using the finite-size scaling relations of the related thermodynamic quantities. Furthermore, the value of correlation length critical exponent ν is obtained using the finite-size scaling relations of the Binder cumulant. For the continuous $Q \to F$ PT, $Q \to F \to Q$ PT in the re-entrant $Q \to F \to Q \to SQ$ PTs and the $Q \to F$ PT in the successive $Q \to F \to SQ$ PT, the estimated values of the critical exponents are equal to universal values ($\beta = 0.31$, $\beta' = 0.55$, $\gamma = \gamma' = 1.25$, $\alpha = \alpha' = 0.12$ and $\nu = 0.64$). The obtained result for the BEG model are compatible with the universal Ising model critical behavior.

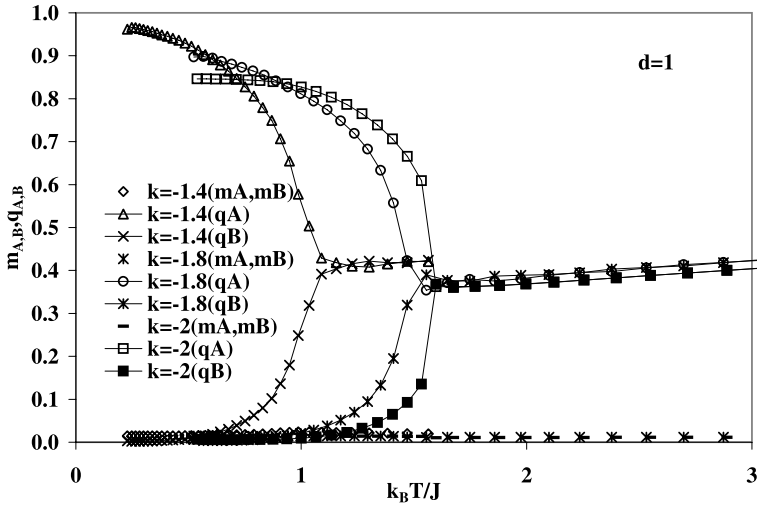

Fig. 12 The temperature dependence of the sublattice order parameters m_A, m_B and q_A, q_B at $d = 1$ for several k values

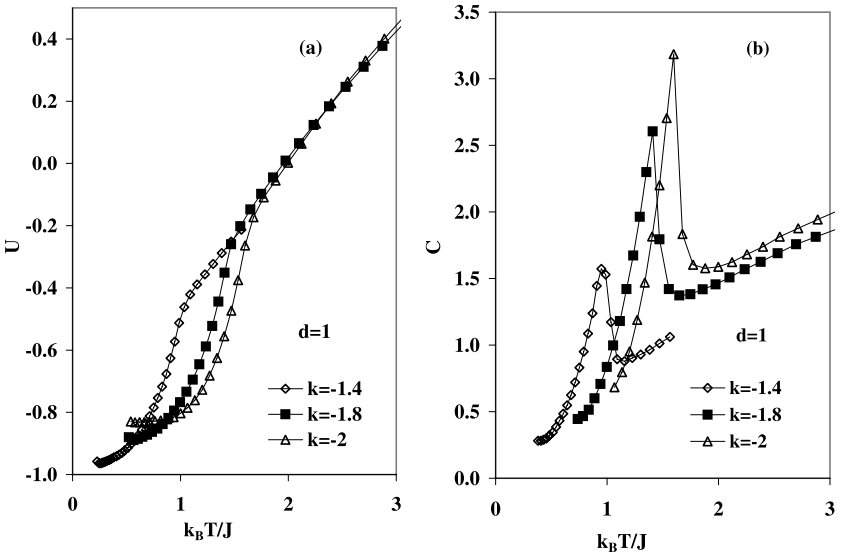

Fig. 13 The temperature dependence of the **a** reduced energy **b** specific heat for $d = 1$ for $k = -1.4$, -1.8 and -2 on a lattice with $L = 18$

Acknowledgements This work is supported by a grant from Gazi University (BAP:05/2003-07).

References

1. Blume, M., Emery, V.J., Griffiths, R.B.: Ising Model for the λ transition and phase separation in He3-He4 mixtures. Phys. Rev. A **4**, 1071 (1971)

2. Lajzerowicz, J., Sivardiere, J.: Spin-1 lattice-gas model. I. Condensation and solidification of a simple fluid. Phys. Rev. A **11**, 2079 (1975)
3. Sivardiere, J., Lajzerowicz, J.: Spin-1 lattice-gas model. I. Condensation and solidification of a simple fluid. Phys. Rev. A **11**, 2090 (1975)
4. Schick, M., Shih, W.H.: Spin-1 model of a microemulsion. Phys. Rev. B **34**, 1797 (1986)
5. Newman, K.E., Dow, J.D.: Zinc-blende—diamond order-disorder transition in metastable crystalline $(GaAs)_{1-x}Ge_{2x}$ alloys. Phys. Rev. B **27**, 7495 (1983)
6. Chen, H.H., Levy, P.M.: Dipole and quadrupole phase transitions in spin-1 models. Phys. Rev. B **7**, 4267 (1973)
7. Hoston, W., Berker, A.N.: Multicritical phase diagrams of the Blume-Emery-Griffiths model with repulsive biquadratic coupling. Phys. Rev. Lett. **67**, 1027 (1991)
8. Buzano, C., Pelizzola, A.: Multicritical points and reentrant phenomenon in the BEG model. Phys. A **189**, 333 (1992)
9. Netz, R.R., Berker, A.N.: Renormalization-group theory of an internal critical-end-point structure: The Blume-Emery-Griffiths model with biquadratic repulsion. Phys. Rev. B **47**, 15019 (1993)
10. Hoston, W., Berker, A.N.: Dimensionality effects on the multicritical phase diagrams of the Blume-Emery-Griffiths model with repulsive biquadratic coupling: Mean-field and Renormalization-group studies. J. Appl. Phys. **70**, 6101 (1991)
11. Kaneyoski, T.: A new disordered phase and its physical contents of the Blume-Emery-Griffiths model. J. Phys. Soc. Jpn. **56**, 4199 (1987)
12. Tucker, J.W.: An effective field study of the staggered quadrupolar phase in the BEG model. J. Magn. Magn. Matter. **183**, 299 (1998)
13. Wang, Y.L., Wentworth, C.: Phase diagrams of three-dimensional Blume–Emery–Griffiths model. J. Appl. Phys. **61**, 4411 (1987)
14. Wang, Y.L., Lee, F., Kimel, J.D.: Phase diagrams of the spin-1 Ising Blume-Emery-Griffiths model: Monte Carlo simulations. Phys. Rev. B **36**, 8945 (1987)
15. Kasono, K., Ono, I.: Re-entrant phase transitions of the Blume-Emery-Griffiths model. Z. Phys. B: Condens. Matter **88**, 205 (1992)
16. Rachadi, A., Benyoussef, A.: Monte Carlo study of the Blume-Emery-Griffiths model at the ferromagnetic-antiquadrupolar-disorder phase interface. Phys. Rev. B **69**, 064423 (2004)
17. Netz, R.R.: New phases and multiple re-entrance of the Blume-Emery-Griffiths model with repulsive biquadratic coupling: Monte Carlo Renormalization-group theory. Europhys. Lett. **17**, 373 (1992)
18. Lapinkas, S., Rosengren, A.: Blume-Emery-Griffiths model on three-dimensional lattices: Consequences for the antiferromagnetic Potts model. Phys. Rev. B **49**, 15190 (1994)
19. Balcerzak, T., Gzik-Szumiata, M.: Magnetic properties of the Blume-Emery-Griffiths model in the vicinity of an antiferromagnetic Potts line. Phys. Rev. B **60**, 9450 (1999)
20. Ekiz, C., Keskin, M.: Multicritical phase diagrams of the Blume-Emery-Griffiths model with repulsive biquadratic coupling including metastable phases. Phys. Rev. B **66**, 054105 (2002)
21. Keskin, M., Ekiz, C., Yalçın, O.: Stable, metastable and unstable solutions of the Blume-Emery-Griffiths model. Phys. A **267**, 392 (1999)
22. Kutlu, B.: The simulation of the 2D ferromagnetic Blume-Capel model on a cellular automaton. Int. J. Mod. Phys. C **12**, 1401 (2001)
23. Kutlu, B., Özkan, A., Seferoğlu, N., Solak, A., Binal, B.: The tricritical behavior of the 3D Blume-Capel model on a cellular automan. Int. J. Mod. Phys. C **16**, 1933 (2005)
24. Seferoğlu, N., Kutlu, B.: Re-entrant phase transitions of the Blume-Emery-Griffiths model for a simple cubic lattice on a cellular automaton. Physica A **374**, 165 (2007)
25. Creutz, M.: Microcanonical Monte Carlo simulation. Phys. Rev. Lett. **50**, 1411 (1983)
26. Aktekin, N.: In: Stauffer, D. (ed.) Annual Reviews of Computational Physics, vol. VII, p. 1. World Scientific, Singapore (2000)
27. Kutlu, B.: The simulation of 2D spin-1 Ising model with positive biquadratic interaction on a cellular automaton. Int. J. Mod. Phys. C **14**, 1305 (2003)
28. Kutlu, B.: Critical behavior of the two-dimensional Ising model with next-nearest-neighbor antiferromagnetik interaction on the Creutz cellular automaton. Phys. A **234**, 807 (1997)
29. Aktekin, N.: The finite-size scaling functions of the four-dimensional Ising model. J. Stat. Phys. **104**, 1397 (2001)
30. Merdan, Z., Günen, A., Mülazimoğlu, G.: Effect of the number of energy levels of a demon for the simulation of the four-dimensional Ising model on the Creutz cellular automaton. Int. J. Mod. Phys. C **16**, 1269 (2005)

31. Aktekin, N., Erkoç, S.: The test of the finite-size scaling relations for the seven-dimensional Ising model on the Creutz cellular automaton. Phys. A **290**, 123 (2001)
32. Aktekin, N., Erkoç, S.: The test of the finite-size scaling relations for the six-dimensional Ising model on the Creutz cellular automaton. Phys. A **284**, 206 (2000)
33. Binder, K.: Z. Phys. B Condens. Matter **43**, 119 (1981)
34. Privman, V.: Finite Size Scaling and Numerical Simulation of Statistical Systems. World Scientific, Singapore (1990)